Published in final edited form as:
Sci Transl Med. 2018 August 15; 10(454): . doi:10.1126/scitranslmed.aan1230.

TGFβ inhibition restores a regenerative response in acute liver injury by suppressing paracrine senescence

Thomas G Bird[1,2,3,*], **Miryam Müller**[1], **Luke Boulter**[2,4], **David F Vincent**[1], **Rachel A Ridgway**[1], **Elena Lopez-Guadamillas**[5], **Wei-Yu Lu**[2], **Thomas Jamieson**[1], **Olivier Govaere**[6], **Andrew D Campbell**[1], **Sofía Ferreira-Gonzalez**[2], **Alicia M Cole**[1], **Trevor Hay**[7], **Kenneth J Simpson**[2], **William Clark**[1], **Ann Hedley**[1], **Mairi Clarke**[8], **Pauline Gentaz**[1], **Colin Nixon**[1], **Steven Bryce**[1], **Christos Kiourtis**[1,9], **Joep Sprangers**[1], **Robert J B Nibbs**[8], **Nico Van Rooijen**[10], **Laurent Bartholin**[11], **Steven R. McGreal**[12], **Udayan Apte**[12], **Simon T Barry**[13], **John P Iredale**[3,14], **Alan R Clarke**[7], **Manuel Serrano**[5,15], **Tania A Roskams**[6], **Owen J Sansom**[1,9], and **Stuart J Forbes**[2,3]

[1]Cancer Research UK Beatson Institute, Glasgow, G61 1BD, UK [2]MRC Centre for Regenerative Medicine, University of Edinburgh, 49 Little France Crescent, Edinburgh, EH16 4SB, UK [3]MRC Centre for Inflammation Research, The Queen's Medical Research Institute, University of Edinburgh, EH164TJ, UK [4]MRC Human Genetics Unit, Institute of Genetics and Molecular Medicine, Edinburgh, EH4 2XU [5]Tumour Suppression Group, Spanish National Cancer Research Centre (CNIO), Madrid 28029, Spain [6]Department of Imaging and Pathology, KU Leuven and University Hospitals Leuven, B-3000 Leuven, Belgium [7]School of Biosciences, Cardiff University, Cardiff, CF10 3AX, UK [8]Institute for Infection Immunity and Inflammation, College of Medical Veterinary and Life Sciences, University of Glasgow, G12 8TA [9]Institute of Cancer Sciences, University of Glasgow, Glasgow G61 1QH, United Kingdom [10]Vrije Universiteit Medical Center (VUMC), Department of Molecular Cell Biology, Van der Boechorststraat 7, 1081 BT Amsterdam, The Netherlands [11]Centre de Recherche en Cancérologie de Lyon (CRCL), UMR INSERM 1052 - CNRS 5286 – Lyon I University UMR S 1052, 69373 LYON Cedex 08, France [12]Department of Pharmacology, Toxicology & Therapeutics, University of Kansas Medical Center (KUMC), Kansas City, KS, USA [13]Oncology IMED, Biotech Unit, AstraZeneca, Cambridge CB2 0AA, UK [14]University of Bristol, Senate House, Tyndall Avenue, Bristol. BS8 1TH, UK [15]Institute for

[*]Dr Thomas G. Bird, Cancer Research UK Beatson Institute, Glasgow, G61 1BD, UK. t.bird@beatson.gla.ac.uk.

Author Contributions:
T.G.B., U.A., M.S., T.A.R., J.P.I., O.J.S. and S.J.F. designed the study. O.G., K.J.S. and T. A. R. collected and analysed human tissue. T.G.B., M.M., R.A.R., T.J., C.K. and S.M. performed *in vivo* experiments. E.L.G. conducted experiments in $p21^{KO}$ mice. L.B. and W.L. conducted experiments using Liposomal Clodronate and transplantation respectively. T.G.B., M.M., D.F.V., S.F.G., A.M.C., T.H., M.C., P.G., C.N., S.B., J.S. and R.J.B.N. performed additional experiments and analysis. A.D.C., A.H. and W.C. performed bioinformatics and statistics. N.V.R., L.B., and S.T.B. provided resources. T.G.B., wrote the manuscript. T.G.B., M.M., M.S., T.A.R., O.J.S and S.J.F. reviewed and edited the manuscript. T.G.B., O.J.S. and S.J.F. provided project administration and T.G.B., A.R.C., U.A., M.S., O.J.S. and S.J.F. raised project funding.

Competing Interested: J.P.I. has consulted for Novartis. M.S. is co-founder and advisor of Senolytic Therapeutics, S.L. (Spain) and Senolytic Therapeutics, Inc. (USA) aimed at developing senolytic therapies. S.T.B. is an AstraZeneca employee and shareholder. The other authors declare no competing interests.

Data and materials availability: The data for this study have been deposited in Geo at NCBI accession number GSE111828. The following materials were provided under Materials Transfer Agreements: AAV8 vector (Penn Vector Core), LSL-TGFβR1-CA mice (INSERM), and AZD12601011 (AstraZeneca).

Overline: Liver Disease

Europe PMC Funders Author Manuscripts

Research in Biomedicine (IRB Barcelona), Barcelona Institute of Science and Technology (BIST), and Catalan Institution for Research and Advanced Studies (ICREA), Barcelona, Spain

Abstract

Liver injury results in rapid regeneration through hepatocyte proliferation and hypertrophy. However, after acute severe injury, such as acetaminophen poisoning, effective regeneration may fail. We investigated how senescence may underlie this regenerative failure. In human acute liver disease, and murine models, p21-dependent hepatocellular senescence was proportionate to disease severity and was associated with impaired regeneration. In an acetaminophen injury mouse model, a transcriptional signature associated with the induction of paracrine senescence was observed within twenty four hours, and was followed by one of impaired proliferation. In mouse genetic models of hepatocyte injury and senescence we observed transmission of senescence to local uninjured hepatocytes. Spread of senescence depended upon macrophage-derived TGFβ1 ligand. In acetaminophen poisoning, inhibition of TGFβ receptor 1 (TGFβR1) improved mouse survival. TGFβR1 inhibition reduced senescence and enhanced liver regeneration even when delivered after the current therapeutic window for acetaminophen poisoning. This mechanism, in which injury-induced senescence impairs liver regeneration, is an attractive therapeutic target for developing treatments for acute liver failure.

Introduction

After moderate liver injury or resection, the liver regenerates efficiently through hepatocyte proliferation (1, 2). However, following severe acute liver injury there is a failure of regeneration and acute liver failure may follow. Acute liver failure can be caused by a variety of insults including viruses, toxins and medical therapy, with the most common single agent in the Western world being acetaminophen (paracetamol) (3). There are approximately 2000 patients affected annually in the US from acute liver failure. Despite its relative rarity, acute liver failure is clinically important, due to its high morbidity and mortality in previously healthy individuals. Outcomes in acute liver failure have improved modestly with advances in supportive care (4). However, once acute liver failure of a defined clinical severity is established no specific medical therapies exist, recovery is unlikely and unless liver transplantation occurs death usually ensues (5). New therapies are needed for the potential treatment window during this progression from acute liver injury to the most severe forms of acute liver failure.

Cells may enter growth arrest in response to stress, which is termed senescence when permanent. Senescence is associated with changes in morphology and lysosomal activity including senescence-associated β-galactosidase (SA-βGal) expression. Senescence is also marked by both a DNA damage response, which includes alterations in chromatin structure (e.g. γH2Ax expression), and also the activation of a dynamic pro-inflammatory senescence-associated secretory phenotype (SASP) including expression of IL1α and TGFβ (6, 7). When senescence results from oncogenic stress it reinforces cell cycle arrest in an autocrine manner (8, 9), activates immune surveillance (10–13) and induces paracrine

senescence via SASP (14, 15). SASP may also modulate fibrosis and regeneration in response to acute tissue injury (11, 16, 17). Hepatocyte senescence involves the induction of genes encoding p53 (*TRP53*), p21 (*WAF1*) and p16 (*INK4A*) (18). It is described in both chronic diseases (19) and steatosis (20), but not in acute liver disease. Fibroblast senescence occurs in the dermis following acute wounding (21) and acute myocardial infarction (22). However, it is not clear whether there is acute epithelial senescence in response to liver injury.

Here, we show that acute liver injury is associated with a suite of senescence markers in previously uninjured hepatocytes. We show that senescence is transmitted between hepatocytes in a feedback loop that is dependent upon TGFβ derived from macrophages. Importantly, targeting TGFβ signaling after acetaminophen-induced injury reduced senescence development and improved both regeneration and survival in a mouse model of acute liver injury and failure.

Results

Acute liver injury results in proportionate acute hepatocellular senescence

Human liver specimens resected at the time of liver transplantation from patients with hyperacute fulminant hepatic failure (less than 1 week from jaundice to encephalopathy, with no prior liver disease) showed expression of various senescence related markers including p21 (Fig. 1A), DcR2, γH2Ax and SA-βGal (Fig. S1). Thus, in liver disease's most severe form a previously healthy human liver develops widespread markers of hepatocellular senescence within days of acute insult. To examine a potential relationship between disease severity and senescence induction, we then analyzed a case series of human diagnostic liver biopsy samples from patients with sub-massive hepatic necrosis. Here, we observed a direct association between hepatic necrosis and hepatocyte senescence as well as an indirect association between necrosis and hepatocellular proliferation (Fig. 1B and S1). Therefore, worsening acute liver injury in humans results in a proportional expression of senescent markers by hepatocytes, associated with a reduced capacity for liver regeneration.

To investigate the functional impact of senescence in acute liver injury, we examined the established murine models of acute liver injury induced by carbon tetrachloride (CCl_4) (23) or acetaminophen (24). Both injury models resulted in expression of senescence markers (p21, SA-βGal and p16) by hepatocytes, demonstrating features of growth arrest (absence of BrdU or Ki67), the DNA damage response (γH2Ax), senescence associated heterochromatic foci (HMGA2) and SASP (IL1α) (Fig. 2A-C and Figs. S2 and S3). We also observed senescence marker expression by hepatocytes in dietary models inducing either hepatocellular steatosis plus injury (CDE diet) or biliary related liver injury (DDC diet) (Fig. S4). In both CCl_4 and acetaminophen induced acute liver injury, expression of senescence markers was maximal two days after initiation and was lost following hepatocellular recovery (Fig. 2D and Figs. S2 and S3 and Table S1). In acetaminophen injury, using unbiased transcriptomics, we confirmed a senescence-associated gene expression signature 24 hours following injury (Fig. 2E and Tables S2 and S3). At 48 hours after acetaminophen injury, we observed p21 expression particularly focused to hepatocytes surrounding the area of receding necrosis at this time of injury resolution (Fig. 2F and S3C). In acute liver injury-

induced senescence, the principal target population is the hepatocyte, however, p21 expression by non-parenchymal cells also occurs (Fig. S2) consistent with the previous report by Krizhanovsky *et al.* (11).

To assess the necessity for p21 in the formation of injury-induced senescence, we performed acetaminophen-induced injury in wildtype and p21-deficient ($p21^{KO}$) mice (Fig. 2G). We measured the proliferative response within the perinecrotic area where p21 was expressed by wildtype hepatocytes. Injury was equivalent between wildtype and $p21^{KO}$ mice (Fig. S3). However, perinecrotic hepatocellular regeneration was increased in $p21^{KO}$ mice compared to wildtype mice (Fig. 2H and Table S1). Furthermore, whilst a negative correlation between injury and regeneration existed in wildtype mice, a positive correlation was observed in $p21^{KO}$ animals (Fig. 2I and Table S1) indicating that in the absence of p21 injury no longer impeded the regenerative response. Together, these data show that hepatocytes can enter a p21-dependent senescent state following acute injury and that this is associated with impaired local regeneration.

TGFβ-dependent senescence transmission between hepatocytes *in vivo*

Rapid entry of the liver parenchyma into senescence following injury may represent a precursor to cell death. However, as we observed increasing expression of senescence markers by hepatocytes during the time of necrosis recession, we explored the hypothesis that ongoing senescence may be a cellular response to adjacent injury and existing senescence. We, and others, have shown that oncogene-induced senescence is not only cell-autonomous but also spreads via paracrine factors (7, 15). Furthermore, transcriptomic analysis revealed a transition between a gene expression signature associated with SASP-induced senescence and one of cell cycle regulation during the induction of senescence following acetaminophen toxicity (Fig. 3A). Thus, we studied the spread of senescence in two independent genetic mouse models of senescence.

Murine Double Minute 2 (*Mdm2*) is a key negative regulator of p53, and the p53/p21 pathway is central to senescence induction. We induced upregulation of p53 in hepatocytes by inducing hepatocyte-specific deletion of *Mdm2* ($\Delta Mdm2^{Hep}$). We achieved this using the AhCre system (25) which expresses Cre recombinase in hepatocytes in response to administration of a xenobiotic chemical (β-naphthoflavone - βNF) rendering Mdm2 inactive. This resulted in hepatocellular injury as we have previously reported (26). In the $\Delta Mdm2^{Hep}$ mouse model we observed a rapid expression of a suite of senescence markers (Fig. S5). Using a mitogen cocktail, consisting of hepatocyte growth factor (HGF) and triodothyronine (T3) (27), we attempted to promote proliferation of senescent hepatocytes in the $\Delta Mdm2^{Hep}$ model, but were unable to do so, unlike in wildtype hepatocytes (Fig. S5). Therefore, these cells appeared to be in a state of functional senescence. Next, we tested p21 dependence of growth arrest in this model. When *Mdm2* was deleted in hepatocytes of $p21^{KO}$ mice, we observed rescue of the growth arrest (Fig. S5). Thus, the $\Delta Mdm2^{Hep}$ model induces acute p21-dependent hepatocellular senescence.

To examine spread of senescence, we utilised reduced titration of βNF to delete *Mdm2* in a subpopulation of hepatocytes (partial $\Delta Mdm2^{Hep}$). By doing so, we aimed to distinguish cell-autonomous and non-cell-autonomous senescence induction in hepatocytes (Fig. 3B).

We define cell-autonomous senescence as being caused through genetic manipulation of that cell (e.g. through *Mdm2* deletion), whereas we consider non-cell-autonomous senescence as an indirect response to environmental senescence and injury in a genetically unmanipulated cell. In the Δ*Mdm2*^{Hep} mouse model, a cell-autonomous senescence was observed with activation of p21/p16 in association with p53 overexpression within a subgroup of the total hepatocyte population (Fig. 3C and Fig. S6). Non-cell-autonomous expression of p21/p16 occurred in a distinct hepatocyte subpopulation in the absence of p53 overexpression. These cells had atypical morphology and more pronounced p21 expression than did their neighbouring p21^{+}/p53^{+} *Mdm2*-deleted hepatocytes.

Next, we examined a potential geographical relationship between non-cell-autonomous p21 expression and regional p53^{+} hepatocytes using a further titrated genetic induction of hepatocyte *Mdm2* deletion. We observed a lower frequency of non-cell-autonomous p21 expression and geographical clustering of non-cell-autonomous p21 expressing hepatocytes in areas dense with hepatocytes overexpressing p53 (Fig. S6).

We then aimed to study senescence transmission from *Mdm2* deleted hepatocytes to local hepatocytes in different mouse models. To exclude any extrahepatic effects of AhCre-mediated recombination (including the intestinal epithelium) (28), we utilised a hepatocyte-specific induction regime using an adeno-associated viral vector, AAV8-thyroxine binding globulin (TBG)-Cre, to induce hepatocyte-specific deletion of *Mdm2* (29). As predicted, AAV8-TBG-Cre induced deletion of *Mdm2* in a subpopulation of hepatocytes (Fig. S6). In this model, non-cell-autonomous p21 expression was also observed (Fig. 3D). We did observe a very low (0.3% hepatocytes) Cre-independent expression of p21 as a result of transfection with the control AAV8 vector (Fig. S6). To test transmission of senescence to wildtype hepatocytes, we utilised a large-scale hepatocyte repopulation model. Using iterative βNF dosing, we found that the livers of AhCre^{+} *Mdm2*$^{fl/fl}$ mice were repopulated by hepatocytes derived from transplanted wildtype GFP-tagged cells (26). Following final βNF dosing and p53 expression by native hepatocytes, transplanted wildtype hepatocytes expressed p21, particularly at the margins of the engrafted nodules (Fig. 3E).

In the Δ*Mdm2*^{Hep} model we observed activation of the TGFβ pathway (Fig. S5). TGFβR1 was expressed by hepatocytes in addition to non-epithelial cells. The TGFβR1 ligand, TGFβ1, was expressed both by non-parenchymal cells and to a lesser degree by hepatocytes. As p21 is a canonical TGFβ signaling target gene and the TGFβ signaling pathway has a role in oncogene-induced paracrine senescence (14, 15), we hypothesised that the TGFβ1 ligand plays a mechanistic role in non-cell-autonomous p21 expression by hepatocytes. To test the functional role of TGFβR1 and TGFβ1 ligand in transmitted senescence, we utilised a model of hepatocyte-specific TGFβ signal pathway activation. Here we used LSL-TGFβR1-CA mice, which possess a genetically inducible constitutively active (CA) TGFβR1 which is expressed upon removal of a stop codon (LSL) by Cre recombinase (30). We activated this model by using hepatocyte-targeted recombination (AAV8-TBG-Cre), and observed TGFβ pathway activation and acute senescence marker induction in hepatocytes. This was accompanied by liver injury and increased paracrine TGFβ1 production (Fig. 3F and S7 and S8). Using this as a further model of senescence induction *in vivo*, we investigated non-cell-autonomous senescence driven specifically by the TGFβ pathway as a

model distinct from *Mdm2* deletion. Using lower titrations of AAV8-TBG-Cre, we induced TGFβ pathway activation and the R26-LSL-tdTomato reporter in approximately 5% of mouse hepatocytes. We observed evidence of non-cell-autonomous spread of senescence to adjacent hepatocytes in response to cell-autonomous TGFβ pathway activation (Fig. 3G). Thus, we observed non-cell-autonomous senescence in mouse models of acute hepatocellular senescence *in vivo* suggesting that senescence can spread within the liver epithelium.

To test the necessity of TGFβ signaling for the transmission of senescence, we returned to the Δ*Mdm2*^{Hep} model. Using SB525334, a small molecule inhibitor of TGFβR1, in the partial Δ*Mdm2*^{Hep} mouse model we observed reduced hepatocellular pSMAD3 without an effect upon hepatocyte Δ*Mdm2*^{Hep} recombination efficiency (Fig. S6). SB525334 treatment of partial Δ*Mdm2*^{Hep} resulted in reduced non-cell-autonomous expression of p21 (Fig. 3H and Table S4), demonstrating that TGFβ signaling was required for the paracrine induction of non-cell-autonomous p21 in this mouse model.

Hepatocyte senescence induced by acute injury is dependent upon macrophage-derived TGFβ

Clinically relevant TGFβ inhibitors are currently available (31). Given our findings of TGFβ-dependent transmitted senescence in the genetic mouse models, we examined the functional role of TGFβR1 signaling in senescence formation in acute liver injury. In human fulminant liver failure, senescent hepatocytes showed TGFβ pathway activity (Fig. 4A). Acetaminophen-induced liver injury in mice was accompanied by elevated TGFβ1 (Fig. 4B and C and Table S5). SMAD7 (a TGFβ pathway target gene) was expressed upon acute liver injury and upregulated by perinecrotic hepatocytes (Fig. 4D and Table S5). These perinecrotic hepatocytes expressed both TGFβR1 and senescence markers adjacent to local TGFβ expression (Fig. 4E and Fig. S10). Therefore, we observed evidence of active TGFβ signaling in senescent hepatocytes adjacent to necrosis following acute liver injury.

Macrophages are a known source of TGFβ ligands, particularly in the context of tissue injury (32). Perinecrotic macrophages in murine acetaminophen-induced liver injury expressed TGFβ1 (Fig. 5A). As both TGFβ and CCL2 (a macrophage chemokine and known SASP component) are associated with severe human acute liver disease (33), we proceeded to examine the functional role of macrophage recruitment and TGFβ expression in senescence induction in our liver injury models. A SASP-related pro-migratory chemokine axis developed in partial Δ*Mdm2*^{Hep} mice with expression of both chemokine ligands and receptors (Fig. S11). CCL2 was expressed by non-parenchymal cells in and around the areas of hepatocellular necrosis in acetaminophen injury (Fig. 5B) prior to an increase in circulating monocytes (Fig. 5C) and then local macrophage accumulation (Fig. 5D and Table S6).

To examine the role of macrophages in non-cell-autonomous senescence, we returned to the Δ*Mdm2*^{Hep} mouse model. Inhibition of leukocyte recruitment via CCL2 blockade in the Δ*Mdm2*^{Hep} model reduced non-cell-autonomous p21 expression and improved hepatocellular regeneration (Fig. 5E and S11 and Table S6). Next, we performed macrophage ablation using liposomal clodronate in the partial Δ*Mdm2*^{Hep} model. This

reduced hepatic *TGFβ1* expression by 87% (Fig. 5F and S11 and Table S6), implying that macrophages are the principal source of the TGFβ1 ligand. Consistent with this hypothesis, both *p21* gene expression and non-cell-autonomous p21 expression were reduced when macrophages were depleted in the partial Δ*Mdm2*^{Hep} mouse model (Fig. 5F and Table S6). To functionally test the role of macrophage-derived TGFβ1 ligand in liver injury, we used myeloid specific *TGFβ1* deletion in the acetaminophen-induced liver injury mouse model (Fig. 5G and S11 and Table S6). This resulted in equivalent injury but improved liver regeneration. Therefore, macrophage-derived TGFβ1 is required for optimal induction of paracrine senescence following acute liver injury in mice.

Inhibition of TGFβR1 signaling impairs senescence induction and improves liver regeneration, function and outcome in acute liver injury

Given the finding of TGFβ-dependent paracrine senescence in the genetic models, we tested whether this effect was also observed in two clinically relevant models of liver injury, the CCL_4 and acetaminophen models. We examined the effect of TGFβ signalling disruption in both acute and chronic CCl_4 liver injury models. In the acute model, we used the TGFβR1 inhibitor AZ12601011 administered twelve hours after administration of 1μl/g CCl_4. (Fig. S12). This resulted in reduced senescence induction, improved liver regeneration and reduced jaundice. In the chronic liver injury model, CCl_4 was given repeatedly over eight weeks in combination with a genetic depletion approach targeting hepatocellular TGFβR1 (Δ*TGFβR1*^{Hep}; Fig. S12). Again, we observed reduced hepatocellular p21 expression and increased hepatocellular proliferation. Next, we examined Δ*TGFβR1*^{Hep} in acute acetaminophen-induced injury (Fig. S13). We observed early necrosis equivalent to controls, but reduced hepatocellular p21 expression by perinecrotic hepatocytes. There was also an altered distribution of hepatocellular regeneration, with marked proliferation by perinecrotic hepatocytes. Accelerated resolution of necrosis was observed in mice lacking hepatocellular *TGFβR1*.

To test the clinical utility of TGFβR1 inhibition, we administered AZ12601011 at the time of a lethal acetaminophen dose (Fig. 6A). TGFβR1 inhibition resulted in marked clinical improvement from 6-16 hours and permitted survival following 525mg/kg acetaminophen dosing (Fig. 6B and Table S7). At the endpoint, vehicle-treated mice showed worsened jaundice compared to their AZ12601011-treated counterparts (Fig. 6C and Table S7).

Conventional treatment of acetaminophen toxicity in humans involves N-acetylcysteine therapy which, to be effective, must be given within eight hours after exposure for humans or four hours for mice (34). Many patients present to medical services too late for this to be effective (35). In order to model delayed treatment, we used small molecule TGFβR1 inhibitors commencing either SB525334 or AZ12601011 treatment of mice twelve hours after acetaminophen administration (Fig. 6D). Additionally, as liver injury peaks prior to treatment administration, this strategy was designed to test whether the improvements in clinical outcome were distinct from the reduced hepatocellular injury we observed with synchronous acetaminophen toxin and therapy administration. With SB525334 treatment, downstream signaling through TGFβR1 was inhibited and necrosis was unchanged (Fig. S14). Liver injury was reduced upon TGFβR1 inhibition (Fig. S14), along with a resolution

of jaundice (Fig. 6E and Table S7). Hepatocellular senescence was reduced by TGFβR1 inhibition (Fig. 6F and Fig. S14 and Table S7) and hepatocellular proliferation increased, both overall and specifically within the perinecrotic area (Fig. 6G and Table S7). During untreated acetaminophen-induced injury an apparent inverse relationship between severity of hepatocellular injury and hepatocellular regeneration was once again observed (Fig. 6H and Fig. 2I and Table S7). Therefore, severe liver injury in the mouse recapitulates the negative correlation between injury and regeneration observed in severe human disease (Fig. 1). In the mouse, this relationship was reversed upon inhibition of TGFβR1, restoring a proportional regenerative response to liver injury, mimicking genetic deletion of *p21*. Using a higher dose of acetaminophen to induce non-fatal liver injury, we tested the second clinical compound AZ12601011 in the delayed treatment mouse model. Here, jaundice was once again improved and was associated with an inhibition of hepatocellular senescence (Fig. 6I and Table S7). These effects were accompanied by reduced local TGFβ pathway activation in perinecrotic hepatocytes (Fig. S14). Therefore, inhibition of TGFβ signaling following acute liver injury reduced hepatocellular senescence and improved liver regeneration and recovery from injury.

Discussion

In contrast to minor forms of acute liver injury where regeneration occurs efficiently, increasingly severe liver injury exhibits regenerative failure and poorer prognosis (4). Validated clinical scoring systems predict the outcomes of patients who will survive versus those in whom liver regeneration will ultimately fail (36), suggesting a tipping-point beyond which recovery is unlikely. The pathophysiological mechanism underlying this remains poorly understood and is a barrier to therapeutic development. Our finding that hepatocyte senescence inhibits liver regeneration may underpin this tipping point. These findings contrast with previous reports in which senescence following injury in other organs may facilitate regeneration (37) and limit fibrosis following liver injury (11).

With our data we provide a mechanistic model whereby injury-induced senescence is amplified by macrophage-dependent paracrine TGFβ signalling (Fig. S15). In our *in vivo* models, we observed the expression of local TGFβ ligand in response to cell intrinsic TGFβR pathway activation. This may represent a paracrine positive-feedback loop reinforcing and amplifying local TGFβ signalling and downstream senescence.

Senescence is challenging to define and study *in vivo*. Hepatocytes in the Δ*Mdm2*^{Hep} mouse model shows functional senescence *in vivo*. They also express a suite of senescence markers (38) including markers of the DNA damage response as well as growth arrest and SASP. Likewise, the acetaminophen-induced liver injury model displays senescence marker expression by hepatocytes. It also possesses a tissue transcriptomic signature matching that of an *in vitro* oncogene-induced senescence model (the IMR90 ER:RAS model) (15). Therefore, we conclude that our two mouse models demonstrate senescence *in vivo*. A similarly rapid senescence program (including TGFβ production, direct Notch target activation and p16 expression) has been observed in oncogene-induced senescence models within 48 hours *in vitro* (7, 39). This is similar to our *in vivo* observations, which were also associated with an early inflammatory signature (e.g. TGFβ, IL6 and NF-κB expression)

within 24 hours post-acetaminophen exposure. In our model, the SASP components TGFβ and IL6 are expressed concurrently within 12 hours of acetaminophen exposure, however, Hoare *et al.* have shown that they appear sequentially in senescence *in vitro* (7). The acute injury-induced senescence described here may represent a generic response to severe tissue injury whereby regional regeneration is inhibited. Our study does not delineate the mechanisms that link hepatocellular injury to senescence initiation. Whether the recently described cGAS-STING driven senescence pathway detecting cytoplasmic chromatin (40) plays a central role in liver injury-induced senescence remains to be studied. Furthermore, the rapid clearance of senescent hepatocytes in our liver senescence models justifies future investigation.

We have recently reported in an *in vivo* model of hepatocyte growth arrest that cholangiocytes, which expand as a ductular reaction, may act as facultative stem cells for generating hepatocytes with replacement of hepatocytes occurring over weeks to months (29). In comparison, resolution of liver injury and architecture in our acetaminophen-induced and CCl_4-induced mouse liver injury models was complete within one week and was not accompanied by a ductular reaction. Future studies are required to test whether inhibition of senescence in chronic liver injury models (e.g. TGFβ inhibition) may affect regeneration from both the hepatocyte and facultative stem cell pools. However, our data in mouse genetic models suggest that when senescence formation is impaired, the ductular expansion including facultative stem cells is also impaired (Fig. S16).

In the chronic liver injury setting, iterative CCl_4-induced fibrosis has been associated with non-parenchymal (myofibroblast) senescence and an impaired fibrotic response to injury (11). Consistent with this previous report, we observed senescence marker expression by non-parenchymal cells both in acute and chronic mouse liver injury models. However, following acute injury, the predominant cells expressing senescence markers were hepatocytes. Our observations are consistent with a requirement for chronic or iterative injury in order to observe persistent populations of non-parenchymal cells with senescence marker expression.

In this study we have investigated TGFβ as a tractable target to interrupt paracrine-induced non-cell-autonomous p21 expression by hepatocytes in the mouse. Our study does not address whether TGFβ inhibition is effective for acute liver injury and failure in man, and further human safety and efficacy studies are required. Additionally, study of other SASP components which may also promote paracrine senescence following liver injury may be worthwhile (15, 41, 42). In acute liver failure, TGFβ is produced in the injured liver (43). TGFβ tonically inhibits hepatocellular regeneration during health; however, changes in TGFβ ligand and receptor sensitivity facilitate regeneration following partial hepatectomy (44, 45). TGFβ is believed to restrict hepatocellular regeneration rather than just acting as a brake during the termination phase of liver regeneration (1, 46). Clinical oncology trials of TGFβR1 or TGFβ inhibitors in humans are currently underway [e.g. NCT02452008, NCT02581787, respectively; see also (31)]. TGFβR2, by acting as a co-receptor of TGFβR1, may serve as a further potential target for drug development. Long-term therapy using TGFβ inhibition raises potential concerns such as carcinogenesis, autoimmunity or cardiac valvulopathies (47). However, these concerns may prove to be less relevant for the

short periods of therapy (<one week) required for acute liver failure, a condition in which the prognosis is otherwise grave. A further relevant concern relates to the potential physiological role for TGFβ in mechanically stabilizing the local environment through a fibrotic response during acute liver injury. We did not observe hemorrhagic transformation (microscopic bleeding into the tissue parenchyma) following TGFβR1 inhibition in our treated mice, but further studies to ensure efficacy and safety of TGFβR1 inhibition are required.

SASP components including chemokines (e.g. CCL2/CCR2 and CX3CL1/CX3CR1) that promote macrophage recruitment and local TGFβ expression within areas of necrosis, are well described in human fulminant hepatic failure (33, 48). Macrophage recruitment in liver injury shares similarities to the p21-dependent recruitment observed during hepatic oncogene-induced senescence (40) and the clearance of early hepatocellular carcinoma (13).

Severe acute hepatic necrosis induces the spread of senescence to remaining viable hepatocytes, which impairs hepatocyte-mediated regeneration. This process is therapeutically modifiable thus providing the potential for developing future therapies to treat this devastating condition.

Materials and Methods

Study design

This study was designed to examine the role of injury-induced senescence in the mammalian liver. With patient consent and ethical approval provided by the ethical committees of the Scottish A research committee and University Hospitals Leuven, we used archival human tissue retrieved as part of routine clinical care. Murine *in vivo* models were used for mechanistic dissection and preclinical compound testing. The n for murine models was based on the predicted variance in the model and was powered to detect 0.05 significance of 30% magnitude; in the event that no predicted variance was inferable from previous work, preliminary experiments were performed using n=3 mice. Animals were randomly assigned to experimental groups prior to experimental readings; no animals were excluded from analysis (two mice in Fig. 6G did not receive BrdU). No blinding was performed during experimental administration of treatments to mice; vehicle controls were used and no bias was applied during husbandry or during tissue harvesting. Histological sections were assigned a randomized blinded code prior to quantification by a separate researcher and the randomization was decoded at the time of final data analysis.

Human tissue

Human liver biopsies from a clinical series of cases of sub-massive hepatic necrosis (but not necessarily progressing to acute liver failure; n= 74; viral hepatitis n= 13, drug-induced hepatitis n= 21 and cryptogenic hepatitis n= 40) were assessed histologically using H&E, CK19, p16 and Ki67 staining and evaluated by an expert pathologist (TR), who also performed cellular quantification using x400 magnification fields. Diagnoses were based on clinical and radiological data and confirmed by histology. Control human tissue was obtained from the Brain Bank, University of Edinburgh, comprising cases of sudden

unexpected death. These cases were reviewed by a pathologist prior to their inclusion as normal control tissue.

Animal Models

Animal welfare conditions have been previously described (26). Briefly, male and female animals were housed in a specific pathogen free environment and kept under standard conditions with a twelve hour day/night cycle and access to food and water *ad libitum*. Eight week old male C57BL/6J mice were purchased from Charles River UK. All animal experiments were carried out under procedural guidelines, severity protocols and within the UK with ethical permission from the Animal Welfare and Ethical Review Body (AWERB) and the Home Office (UK); or in CNIO Spain performed according to protocols 193 approved by the Institute of Health 'Carlos III' Ethics Committee for Research and Animal Welfare (CEIyBA) and 194 approved by the Autonomous Community of Madrid. As described previously (26), $AhCre^{+/WT}$ mice were crossed with both $Mdm2^{fl/fl}$ and $Mdm2^{fl/+}$ mice to generate $AhCre^{+}$ $Mdm2^{fl/fl}$ and $AhCre^{WT}$ $Mdm2^{fl/fl}$ and $AhCre^{+}$ $Mdm2^{fl/+}$ controls and then subsequently crossed with $p21^{KO}$ (49) and $TGF\beta R1^{fl/fl}$ (50) animals. LysMCre mice were crossed with $TGF\beta1^{fl/fl}$ animals. Litters from $LysMCre^{het}$ $TGF\beta1^{fl/fl}$ x $LysMCre^{WT}$ $TGF\beta1^{fl/fl}$ crosses were used for experimental and control animals. Power calculations were not routinely performed, however, animal numbers were chosen to reflect the expected magnitude of response taking into account the variability observed in previous experiments. Genotyping, BrdU administration and i.p. injection of β-Napthoflavone (βNF, Sigma UK) at 10-80mg/kg were performed as previously described (26, 51), with BrdU given two hours prior to tissue harvest. AAV8 recombination was performed as previously described (52). Briefly, viral particles ($6.4x10^8$, $2x10^{11}$ or $2.5x10^{11}$ genetic copies (GC)/ mouse as specified) of AAV8.TBG.PI.Cre.rBG (UPenn Vector Core, Catalogue number: AV-8-PV1091) were injected via tail vein in 100μL PBS into male $AhCre^{WT}$ $Mdm2^{fl/fl}$, LSL-TGFβR1-CA^{Hom} (30, 53) or wildtype mice. Control male $AhCre^{WT}$ $Mdm2^{fl/fl}$ or LSL-TGFβR1-CA^{Hom} mice received equal AAV8.TBG.PI.Null.bGH (UPenn Vector Core, Catalogue number: AV-8-PV0148) injection. Cell transplantation was performed as previously described (26), AhCre $Mdm2^{fl/fl}$ recipient mice received 10mg/kg i.p. βNF 4 days prior to cell transplant of $5x10^6$ GFP expressing cells suspended in 200μL of PBS and injected intrasplenically after laparotomy. Transplanted $7\text{-}AAD^{-}CD31^{-}CD45^{-}Ter119^{-}EpCAM^{+}CD24^{+}CD133^{+}$ hepatic progenitor cells from wildtype mice fed the CDE diet were transfected using 1μg of vector with a puromycin resistant CAG-GFP prior to transplantation. The transplantation control group received 200μL PBS only. Recipient mice received intraperitoneal injections of 20mg/kg βNF every ten days after transplantation to induce persistent liver injury. Mice were sacrificed and the livers were harvested twelve weeks after cell transplantation. HGF (250μg/kg, R and D technologies) was administered via tail vein injection. Triodothyronine (T3, Sigma) was dissolved in solution (0.01M NaOH, 0.9M NaCl) at 0.4g/l. This solution was then neutralized with 2M HCl upto just prior to T3 precipitation and stored at -20°C. T3 was administered at 4mg/kg to mice via subcutaneous injection. CDE and DDC-supplemented dietary protocols were as previously described (54). 200μl of clodronate liposomes or control PBS were injected i.v. as previously described (54). TGFβR1 antagonists; SB525334 (Tocris) was given at 10mg/kg twice daily in 10% polyethylene glycol, 5% DMSO, 85% saline vehicle by gavage; AZ12601011 (AstraZeneca)

(47) was given at 50mg/kg twice daily in 0.5% HPMC / 0.1% Tween vehicle by gavage. Acetaminophen was prepared as previously described (8) and delivered at 350mg/kg or 450mg/kg by single i.p. injection of 20μl/g following a ten hour fast. 525mg/kg acetaminophen was administered by injection of 30μl/g. CCl_4 was delivered by weekly i.p. injection for eight weeks at 0.75ml/kg or by single dose at 1ml/kg 1:3 in corn oil. CCL2 inhibitory antibody (#AF-4679-NA, R and D Systems) was administered (10μg per injection) daily for four days by tail vein injection of a 100μg/ml stock diluted in PBS.

Animal tissue harvesting and serum analysis

Mice were killed by CO_2 inhalation or cervical dislocation and blood harvested by cardiac puncture. Organs were harvested and stored in paraffin blocks following fixation in 10% formalin (in PBS) for 18 hours prior to embedding. Blood hematology was performed using an IDEXX ProCyte Dx analyzer on blood collected in EDTA. Serum analysis used commercial kits according to manufacturer's instructions for Alanine transaminase (ALT; Alpha Laboratories Ltd, UK), microalbumin (Olympus Diagnostics Lt, UK), Aspartate Aminotransferase (AST) and Alkaline Phosphatase (Alk Phos; both Randox Laboratories, UK).

Immunohistochemistry and in situ hybridization

Three μm thick paraffin sections were stained for BrdU, p16, HMGA2, γH2Ax, DcR2 and pSMAD3 (AB6326 – clone BU1/75, AB54210 – clone 2D9A12, AB52039, AB81299 – clone EP854(2)Y, AB108421 – clone EPR3588(2) and AB52903 – clone EP823Y respectively Abcam, UK), p53 (VP-P956-clone CM5, Vectorn), p21 (Clones BMK-2202, Santa Cruz and HUGO 291H), Ki67 (M7249 - clone TEC-3 Dako), pSMAD2/3, pSMAD2 (Cell Signalling #8828 – clone D26F4, #3101), CYP2D6 (Generous gift from Prof R Wolfe, University of Dundee) and the ductular cell marker panCK (Z0622 Dako), Species isotype (Santa Cruz) staining controls were routinely performed. Detection was performed with DAB (DAKO) followed by counterstaining with Haematoxylin or alternatively with Alexa 488, 555 or 650 (A21206, A21434A21436/S32355 and A21448 respectively; Invitrogen, UK) with a DAPI containing Vectashield mounting media (Vector, UK). Histochemical detection of senescence-associated β-galactosidase (SA-βG) was performed as previously described (55). In situ mRNA hybridization was performed using RNAscope LS probes for *TGFβ1*, *TGFβR1*, *CCL2*, *SMAD7* and *PPIB* control (407758, 406208, 469608, 429418 and 313918); Advanced Cell Diagnostics) as per the manufacturer's instructions.

ELISA for murine TGFβ1 ligand was performed using Mouse/Rat/Porcine/Canine TGF-beta 1 Quantikine ELISA Kit (R and D system) according to the manufacturer's protocol. Whole liver tissue samples were homogenized in RIPA-Buffer (50mM Tris, 150 mM NaCl, 1% Triton x-100, 0.5% Deoxycholate, 0.1% SDS) supplemented with NaF, protease- and phosphatase-inhibitors and cleared by centrifugation. Protein concentration was determined by BCA Assay (Thermo Scientific #23225). The samples were diluted 1:4. To allow TGFβ activation 20ul of 1M HCL and 20ul of 1.2M NaOH/0,5M HEPES were added to each 100ul sample. Optical density was measured using Safire II microplate reader (TECAN) at 450 nm (reference wavelength 540nm).

Microscopy and cell counting

Images were obtained on a Zeiss Axiovert 200 microscope using a Zeiss Axiocam MRc camera. Cell counts were performed manually on blinded slides and consecutive non-overlapping fields at x200 magnification. Perinecrotic hepatocytes were defined as those contacting the area of necrosis. Confocal image analysis was performed using a Leica SP5 system with the pinhole set to 1 airy unit. DAPI, Alexafluor 488 and 555 were detected using band paths of 415-480, 495-540 and 561-682nm for 405, 488 543nm lasers respectively. Serial sections were aligned manually in Adobe Photoshop CS5; images were colour deconvoluted using imageJ using haematoxylin/DAB settings (version 1.5). For RNAscope and quantification of necrosis slides were scanned on an SCN400F slide scanner (Leica, Milton Keynes, UK) and the files analysed using Halo v2.0 Image Analysis Software (Indica Labs, Corrales, NM, USA) as previously described. For perinecrotic SMAD7 quantification, perinecrotic and uninjured pericentral areas were manually defined by drawing a ring (200μm radius from vein or necrosis) around ten centrilobular structures per sample. Results are expressed as probe copies/area for RNAscope. Necrosis was defined after validation of classifier definition of healthy liver, haemorrhagic necrosis and non-haemorrhagic necrosis with results expressed as % area necrosis. All scale bars = 50μm.

Real time PCR and gene expression analysis

Total RNA was extracted from 30-50mg tissue samples previously stored in RNAlater at -80°C, using a combination of TRIzol™ reagent (Invitrogen) and Qiagen RNeasy Mini system (Qiagen, UK) according to both manufacturers' instructions. gDNA decontamination, reverse transcription and real time PCR were performed using reagents and primers (Quantifast and Quantitect respectively, Qiagen, UK) on an ABI Prism 7500 cycler, except for chemokine/chemokine receptor analysis which was performed as previously described (56). Data were collected using the LightCycler system following normalization to the housekeeping gene peptidylprolyl isomerase A (*Ppia*); or *Gapdh* for chemokine/chemokine receptor data. All samples were run in triplicates.

RNAseq analysis

Total RNA was extracted from 30-50mg tissue samples as described above. Purified RNA was tested on an Agilent 2200 Tapestation using RNA screentape. Libraries for cluster generation and DNA sequencing were prepared following an adapted method from Fisher et al.(57) using Illumina TruSeq Stranded mRNA LT Kit, Quality and quantity of the DNA libraries was assessed on a Agilent 2200 Tapestation (D1000 screentape) and Qubit (Thermo Fisher Scientific) respectively. The libraries were run on the Illumina Next Seq 500 using the High Output 75 cycles kit (2x36cycles, paired end reads, single index). Quality checks on the raw RNASeq data files were done using fastqc version 0.10.1 and fastq_screen version 0.4.2. RNASeq reads were aligned to the GRCm38 (58) version of the mouse genome using tophat2 version 2.1.0 (59) with Bowtie version 2.2.6.0 (60). Expression values were determined and statistically analysed by a combination of HTSeq version 0.5.4p3, the R 3.4.2 environment, utilizing packages from the Bioconductor data analysis suite and differential gene expression analysis based on the negative binomial distribution using DESeq2 (61). Gene set enrichment analysis was performed using the Broad Institute Online

Platform. An OIS signature was defined by the top 100 upregulated gene in the IMR90 ER:RAS model (15).

Statistical analysis

Prism software (GraphPad Software, Inc) was used for all statistical analyses; t tests were used for normally distributed samples (D'Agostino Pearson omnibus test was used to assess Gaussian distribution) with Welch's correction if variances differed (F test). One or two way ANOVA was used to compare multiple (>2) samples or groups, respectively. Mean hepatic progenitor cells per x200 magnification field from 30 fields for each mouse were compared. Data are presented as mean +/- SEM throughout; n refers to biological replicates in all instances unless otherwise stated.

Supplementary Material

Refer to Web version on PubMed Central for supplementary material.

Acknowledgments

We thank Professor Lozano (Department of Cancer Genetics, University of Texas) for *Mdm2*^{fl} mice and Dr Ana Sofia Rocha for constructive input into experimental design. Cl2MDP (or clodronate) was a gift of Roche Diagnostics GmbH, Mannheim, Germany. We thank CRUK Beatson Histological services for their assistance. We acknowledge the use of the gene set enrichment analysis, GSEA software, and Molecular Signature Database (MSigDB) (62)

Funding: TGB is funded by the Wellcome Trust (WT081604AIA and WT107492Z). SJF is funded by an MRC project grant (G1000868), the Wellcome Trust, The Jules Thorn Trust and Scottish Enterprise. JPI is supported by an MRC programme grant. OS is supported by CRUK Grant number: A12481. UA is supported by NIH grant # R01 DK98414.

References

1. Michalopoulos GK. Liver regeneration. J Cell Physiol. 2007; 213:286–300. [PubMed: 17559071]
2. Overturf K, al-Dhalimy M, Ou CN, Finegold M, Grompe M. Serial transplantation reveals the stem-cell-like regenerative potential of adult mouse hepatocytes. Am J Pathol. 1997; 151:1273–1280. [PubMed: 9358753]
3. Bernal W, Wendon J. Acute Liver Failure. New England Journal of Medicine. 2013; 369:2525–2534. [PubMed: 24369077]
4. Reuben A, Tillman H, Fontana RJ, Davern T, McGuire B, Stravitz RT, Durkalski V, Larson AM, Liou I, Fix O, Schilsky M, et al. Outcomes in Adults With Acute Liver Failure Between 1998 and 2013: An Observational Cohort Study. Ann Intern Med. 2016; 164:724–732. [PubMed: 27043883]
5. O'Grady JG, Alexander GJ, Hayllar KM, Williams R. Early indicators of prognosis in fulminant hepatic failure. Gastroenterology. 1989; 97:439–445. [PubMed: 2490426]
6. Coppe JP, Patil CK, Rodier F, Sun Y, Munoz DP, Goldstein J, Nelson PS, Desprez PY, Campisi J. Senescence-associated secretory phenotypes reveal cell-nonautonomous functions of oncogenic RAS and the p53 tumor suppressor. PLoS biology. 2008; 6:2853–2868. [PubMed: 19053174]
7. Hoare M, Ito Y, Kang TW, Weekes MP, Matheson NJ, Patten DA, Shetty S, Parry AJ, Menon S, Salama R, Antrobus R, et al. NOTCH1 mediates a switch between two distinct secretomes during senescence. Nat Cell Biol. 2016; 18:979–992. [PubMed: 27525720]
8. Henderson NC, Pollock KJ, Frew J, Mackinnon AC, Flavell RA, Davis RJ, Sethi T, Simpson KJ. Critical role of c-jun (NH2) terminal kinase in paracetamol-induced acute liver failure. Gut. 2007; 56:982–990. [PubMed: 17185352]
9. Yingling JM, Blanchard KL, Sawyer JS. Development of TGF-beta signalling inhibitors for cancer therapy. Nat Rev Drug Discov. 2004; 3:1011–1022. [PubMed: 15573100]

10. Kang TW, Yevsa T, Woller N, Hoenicke L, Wuestefeld T, Dauch D, Hohmeyer A, Gereke M, Rudalska R, Potapova A, Iken M, et al. Senescence surveillance of pre-malignant hepatocytes limits liver cancer development. Nature. 2011; 479:547–551. [PubMed: 22080947]
11. Krizhanovsky V, Yon M, Dickins RA, Hearn S, Simon J, Miething C, Yee H, Zender L, Lowe SW. Senescence of activated stellate cells limits liver fibrosis. Cell. 2008; 134:657–667. [PubMed: 18724938]
12. Reimann M, Lee S, Loddenkemper C, Dorr JR, Tabor V, Aichele P, Stein H, Dorken B, Jenuwein T, Schmitt CA. Tumor stroma-derived TGF-beta limits myc-driven lymphomagenesis via Suv39h1-dependent senescence. Cancer Cell. 2010; 17:262–272. [PubMed: 20227040]
13. Xue W, Zender L, Miething C, Dickins RA, Hernando E, Krizhanovsky V, Cordon-Cardo C, Lowe SW. Senescence and tumour clearance is triggered by p53 restoration in murine liver carcinomas. Nature. 2007; 445:656–660. [PubMed: 17251933]
14. Hubackova S, Krejcikova K, Bartek J, Hodny Z. IL1- and TGFbeta-Nox4 signaling, oxidative stress and DNA damage response are shared features of replicative, oncogene-induced, and drug-induced paracrine 'bystander senescence'. Aging. 2012; 4:932–951. [PubMed: 23385065]
15. Acosta JC, Banito A, Wuestefeld T, Georgilis A, Janich P, Morton JP, Athineos D, Kang T-W, Lasitschka F, Andrulis M. A complex secretory program orchestrated by the inflammasome controls paracrine senescence. Nature Cell Biology. 2013
16. Kong X, Feng D, Wang H, Hong F, Bertola A, Wang FS, Gao B. Interleukin-22 induces hepatic stellate cell senescence and restricts liver fibrosis in mice. Hepatology. 2012; 56:1150–1159. [PubMed: 22473749]
17. Lujambio A, Akkari L, Simon J, Grace D, Tschaharganeh DF, Bolden JE, Zhao Z, Thapar V, Joyce JA, Krizhanovsky V, Lowe SW. Non-cell-autonomous tumor suppression by p53. Cell. 2013; 153:449–460. [PubMed: 23562644]
18. Teoh N, Pyakurel P, Dan YY, Swisshelm K, Hou J, Mitchell C, Fausto N, Gu Y, Farrell G. Induction of p53 Renders ATM-Deficient Mice Refractory to Hepatocarcinogenesis. Gastroenterology. 2010; 138:1155–1165. [PubMed: 19919837]
19. Aravinthan AD, Alexander GJ. Senescence in chronic liver disease: Is the future in aging? J Hepatol. 2016; 65:825–834. [PubMed: 27245432]
20. Ogrodnik M, Miwa S, Tchkonia T, Tiniakos D, Wilson CL, Lahat A, Day CP, Burt A, Palmer A, Anstee QM, Grellscheid SN, et al. Cellular senescence drives age-dependent hepatic steatosis. Nat Commun. 2017; 8
21. Jun JI, Lau LF. The matricellular protein CCN1 induces fibroblast senescence and restricts fibrosis in cutaneous wound healing. Nature cell biology. 2010; 12:676–685. [PubMed: 20526329]
22. Zhu F, Li Y, Zhang J, Piao C, Liu T, Li HH, Du J. Senescent cardiac fibroblast is critical for cardiac fibrosis after myocardial infarction. PloS one. 2013; 8:e74535. [PubMed: 24040275]
23. Font-Burgada J, Shalapour S, Ramaswamy S, Hsueh B, Rossell D, Umemura A, Taniguchi K, Nakagawa H, Valasek MA, Ye L, Kopp JL, et al. Hybrid Periportal Hepatocytes Regenerate the Injured Liver without Giving Rise to Cancer. Cell. 2015; 162:766–779. [PubMed: 26276631]
24. McGill MR, Sharpe MR, Williams CD, Taha M, Curry SC, Jaeschke H. The mechanism underlying acetaminophen-induced hepatotoxicity in humans and mice involves mitochondrial damage and nuclear DNA fragmentation. The Journal of clinical investigation. 2012; 122:1574–1583. [PubMed: 22378043]
25. Ireland H, Kemp R, Houghton C, Howard L, Clarke AR, Sansom OJ, Winton DJ. Inducible Cre-mediated control of gene expression in the murine gastrointestinal tract: effect of loss of beta-catenin. Gastroenterology. 2004; 126:1236–1246. [PubMed: 15131783]
26. Lu W-Y, Bird TG, Boulter L, Tsuchiya A, Cole AM, Hay T, Guest RV, Wojtacha D, Man TY, Mackinnon A, Ridgway RA, et al. Hepatic progenitor cells of biliary origin with liver repopulation capacity. Nat Cell Biol. 2015; 17:971–983. [PubMed: 26192438]
27. Forbes SJ, Themis M, Alison MR, Shiota A, Kobayashi T, Coutelle C, Hodgson HJ. Tri-iodothyronine and a deleted form of hepatocyte growth factor act synergistically to enhance liver proliferation and enable in vivo retroviral gene transfer via the peripheral venous system. Gene Ther. 2000; 7:784–789. [PubMed: 10822305]

28. Valentin-Vega YA, Okano H, Lozano G. The intestinal epithelium compensates for p53-mediated cell death and guarantees organismal survival. Cell death and differentiation. 2008; 15:1772–1781. [PubMed: 18636077]
29. Raven A, Lu WY, Man TY, Ferreira-Gonzalez S, O'Duibhir E, Dwyer BJ, Thomson JP, Meehan RR, Bogorad R, Koteliansky V, Kotelevtsev Y, et al. Cholangiocytes act as facultative liver stem cells during impaired hepatocyte regeneration. Nature. 2017; 547:350–354. [PubMed: 28700576]
30. Bartholin L, Cyprian FS, Vincent D, Garcia CN, Martel S, Horvat B, Berthet C, Goddard-Leon S, Treilleux I, Rimokh R, Marie JC. Generation of mice with conditionally activated transforming growth factor beta signaling through the TbetaRI/ALK5 receptor. Genesis. 2008; 46:724–731. [PubMed: 18821589]
31. Neuzillet C, Tijeras-Raballand A, Cohen R, Cros J, Faivre S, Raymond E, de Gramont A. Targeting the TGFβ pathway for cancer therapy. Pharmacology & Therapeutics. 2015; 147:22–31. [PubMed: 25444759]
32. Fadok VA, Bratton DL, Konowal A, Freed PW, Westcott JY, Henson PM. Macrophages that have ingested apoptotic cells in vitro inhibit proinflammatory cytokine production through autocrine/paracrine mechanisms involving TGF-beta, PGE2, and PAF. Journal of Clinical Investigation. 1998; 101:890. [PubMed: 9466984]
33. Antoniades CG, Quaglia A, Taams LS, Mitry RR, Hussain M, Abeles R, Possamai LA, Bruce M, McPhail M, Starling C, Wagner B, et al. Source and characterization of hepatic macrophages in acetaminophen-induced acute liver failure in humans. Hepatology (Baltimore, Md.). 2012; 56:735–746.
34. James LP, McCullough SS, Lamps LW, Hinson JA. Effect of N-acetylcysteine on acetaminophen toxicity in mice: relationship to reactive nitrogen and cytokine formation. Toxicol Sci. 2003; 75:458–467. [PubMed: 12883092]
35. Ferner RE, Dear JW, Bateman DN. Management of paracetamol poisoning. BMJ (Clinical research ed.). 2011; 342
36. Wlodzimirow KA, Eslami S, Chamuleau RA, Nieuwoudt M, Abu-Hanna A. Prediction of Poor Outcome in Patients with Acute Liver Failureâ€"Systematic Review of Prediction Models. PLoS One. 2012; 7:e50952. [PubMed: 23272081]
37. Munoz-Espin D, Serrano M. Cellular senescence: from physiology to pathology. Nat Rev Mol Cell Biol. 2014; 15:482–496. [PubMed: 24954210]
38. Collado M, Serrano M. Senescence in tumours: evidence from mice and humans. Nature reviews Cancer. 2010; 10:51–57. [PubMed: 20029423]
39. Jeanblanc M, Ragu S, Gey C, Contrepois K, Courbeyrette R, Thuret JY, Mann C. Parallel pathways in RAF-induced senescence and conditions for its reversion. Oncogene. 2011; 31:3072. [PubMed: 22020327]
40. Dou Z, Ghosh K, Vizioli MG, Zhu J, Sen P, Wangensteen KJ, Simithy J, Lan Y, Lin Y, Zhou Z, Capell BC, et al. Cytoplasmic chromatin triggers inflammation in senescence and cancer. Nature. 2017; 550:402. [PubMed: 28976970]
41. Herranz N, Gallage S, Mellone M, Wuestefeld T, Klotz S, Hanley CJ, Raguz S, Acosta JC, Innes AJ, Banito A, Georgilis A, et al. mTOR regulates MAPKAPK2 translation to control the senescence-associated secretory phenotype. Nature cell biology. 2015
42. Laberge RM, Sun Y, Orjalo AV, Patil CK, Freund A, Zhou L, Curran SC, Davalos AR, Wilson-Edell KA, Liu S, Limbad C, et al. MTOR regulates the pro-tumorigenic senescence-associated secretory phenotype by promoting IL1A translation. Nature cell biology. 2015; 17:1049–1061. [PubMed: 26147250]
43. Takiya S, Tagaya T, Takahashi K, Kawashima H, Kamiya M, Fukuzawa Y, Kobayashi S, Fukatsu A, Katoh K, Kakumu S. Role of transforming growth factor beta 1 on hepatic regeneration and apoptosis in liver diseases. J Clin Pathol. 1995; 48:1093–1097. [PubMed: 8567993]
44. Hu J, Srivastava K, Wieland M, Runge A, Mogler C, Besemfelder E, Terhardt D, Vogel MJ, Cao L, Korn C, Bartels S, et al. Endothelial cell-derived angiopoietin-2 controls liver regeneration as a spatiotemporal rheostat. Science. 2014; 343:416–419. [PubMed: 24458641]
45. Houck KA, Michalopoulos GK. Altered responses of regenerating hepatocytes to norepinephrine and transforming growth factor type beta. J Cell Physiol. 1989; 141:503–509. [PubMed: 2574179]

46. Oe S, Lemmer ER, Conner EA, Factor VM, Leveen P, Larsson J, Karlsson S, Thorgeirsson SS. Intact signaling by transforming growth factor beta is not required for termination of liver regeneration in mice. Hepatology (Baltimore, Md.). 2004; 40:1098–1105.
47. Anderton MJ, Mellor HR, Bell A, Sadler C, Pass M, Powell S, Steele SJ, Roberts RR, Heier A. Induction of heart valve lesions by small-molecule ALK5 inhibitors. Toxicol Pathol. 2011; 39:916–924. [PubMed: 21859884]
48. Sasaki M, Miyakoshi M, Sato Y, Nakanuma Y. Modulation of the microenvironment by senescent biliary epithelial cells may be involved in the pathogenesis of primary biliary cirrhosis. Journal of hepatology. 2010; 53:318–325. [PubMed: 20570384]
49. Cole AM, Ridgway RA, Derkits SE, Parry L, Barker N, Clevers H, Clarke AR, Sansom OJ. p21 loss blocks senescence following Apc loss and provokes tumourigenesis in the renal but not the intestinal epithelium. EMBO Mol Med. 2010; 2:472–486. [PubMed: 20976827]
50. Larsson J, Goumans M-J, Sjostrand LJ, van Rooijen MA, Ward D, Leveen P, Xu X, ten Dijke P, Mummery CL, Karlsson S. Abnormal angiogenesis but intact hematopoietic potential in TGF-{beta} type I receptor-deficient mice. Science Signaling. 2001; 20:1663.
51. Lu WY, Bird TG, Boulter L, Tsuchiya A, Cole AM, Hay T, Guest RV, Wojtacha D, Man TY, Mackinnon A, Ridgway RA, et al. Hepatic progenitor cells of biliary origin with liver repopulation capacity. Nature cell biology. 2015
52. Yanger K, Knigin D, Zong Y, Maggs L, Gu G, Akiyama H, Pikarsky E, Stanger BZ. Adult hepatocytes are generated by self-duplication rather than stem cell differentiation. Cell stem cell. 2014; 15:340–349. [PubMed: 25130492]
53. Vincent DF, Kaniewski B, Powers SE, Havenar-Daughton C, Marie JC, Wotton D, Bartholin L. A rapid strategy to detect the recombined allele in LSL-TbetaRICA transgenic mice. Genesis. 2010; 48:559–562. [PubMed: 20645310]
54. Boulter L, Govaere O, Bird TG, Radulescu S, Ramachandran P, Pellicoro A, Ridgway R, Seo SS, Spee B, Van Rooijen N, Sansom OJ, et al. Macrophage-derived Wnt opposes Notch signaling to specify hepatic progenitor cell fate in chronic liver disease. Nat Med. 2012
55. Debacq-Chainiaux F, Erusalimsky JD, Campisi J, Toussaint O. Protocols to detect senescence-associated beta-galactosidase (SA-betagal) activity, a biomarker of senescent cells in culture and in vivo. Nat Protoc. 2009; 4:1798–1806. [PubMed: 20010931]
56. Jamieson T, Clarke M, Steele CW, Samuel MS, Neumann J, Jung A, Huels D, Olson MF, Das S, Nibbs RJ, Sansom OJ. Inhibition of CXCR2 profoundly suppresses inflammation-driven and spontaneous tumorigenesis. The Journal of clinical investigation. 2012; 122:3127–3144. [PubMed: 22922255]
57. Fisher S, Barry A, Abreu J, Minie B, Nolan J, Delorey TM, Young G, Fennell TJ, Allen A, Ambrogio L, Berlin AM, et al. A scalable, fully automated process for construction of sequence-ready human exome targeted capture libraries. Genome biology. 2011; 12:R1. [PubMed: 21205303]
58. Church DM, Schneider VA, Graves T, Auger K, Cunningham F, Bouk N, Chen HC, Agarwala R, McLaren WM, Ritchie GR, Albracht D, et al. Modernizing reference genome assemblies. PLoS biology. 2011; 9:e1001091. [PubMed: 21750661]
59. Kim D, Pertea G, Trapnell C, Pimentel H, Kelley R, Salzberg SL. TopHat2: accurate alignment of transcriptomes in the presence of insertions, deletions and gene fusions. Genome biology. 2013; 14:R36. [PubMed: 23618408]
60. Langmead B, Salzberg SL. Fast gapped-read alignment with Bowtie 2. Nature methods. 2012; 9:357–359. [PubMed: 22388286]
61. Love MI, Huber W, Anders S. Moderated estimation of fold change and dispersion for RNA-seq data with DESeq2. Genome biology. 2014; 15:550. [PubMed: 25516281]
62. Subramanian A, Tamayo P, Mootha VK, Mukherjee S, Ebert BL, Gillette MA, Paulovich A, Pomeroy SL, Golub TR, Lander ES, Mesirov JP. Gene set enrichment analysis: a knowledge-based approach for interpreting genome-wide expression profiles. Proceedings of the National Academy of Sciences of the United States of America. 2005; 102:15545–15550. [PubMed: 16199517]

Europe PMC Funders Author Manuscripts

One Sentence Summary

Inhibiting acute injury-induced senescence mediated by TGFβ signaling in regenerative epithelium improves liver regeneration.

Europe PMC Funders Author Manuscripts

Accessible Summary: Freeing the chains holding back liver regeneration

The liver is a paradigm of organ regeneration, however regeneration may fail in a previously normal liver following acute severe injury such as acetaminophen poisoning. We show that a process which prevents proliferation termed senescence, which is classically associated with aging and carcinogenesis, stops the liver's regenerative cells after acute injury. This senescence can be spread from cell to cell by the signaling molecule TGFβ. When TGFβ signaling is inhibited during acetaminophen poisoning in mice senescence is impeded, regeneration accelerates, and survival is improved. Therefore targeting senescence induced by acute tissue injury is an attractive therapeutic approach to improve regeneration.

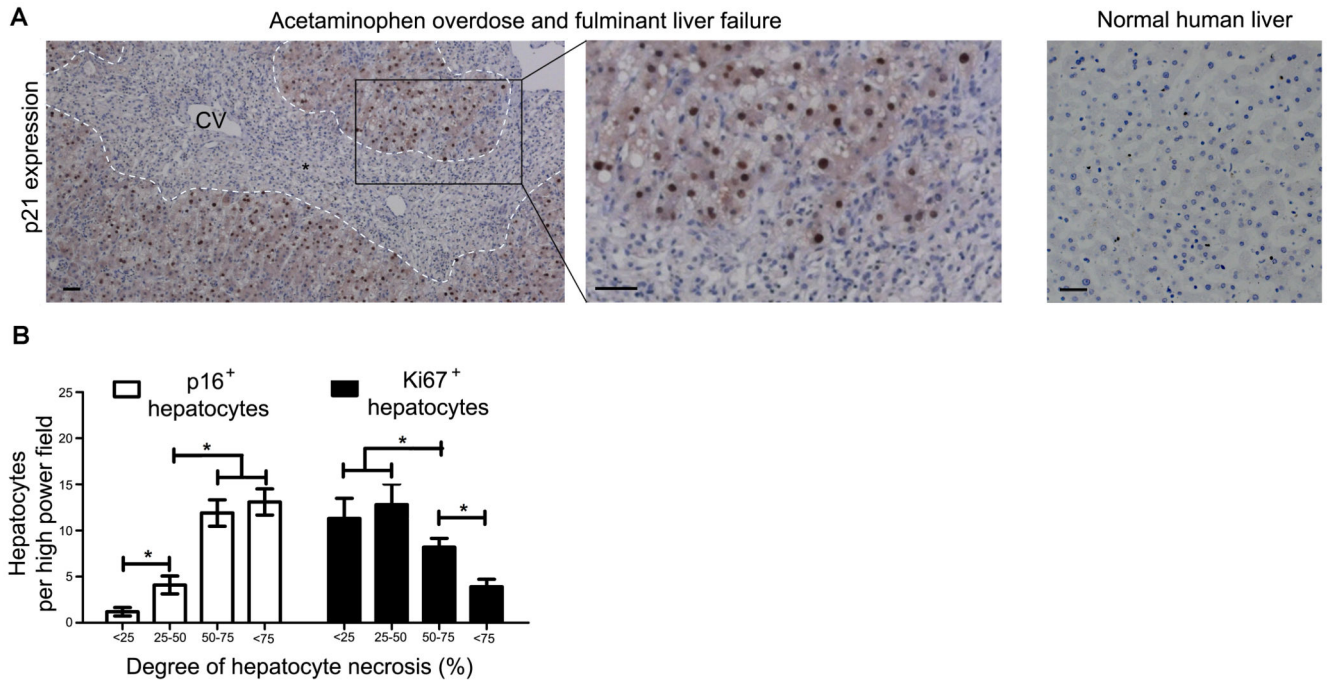

Fig. 1. Human liver necrosis causes acute hepatocellular senescence.

(**A**) Shown are representative images of sections of explanted human liver following liver transplantation for severe acetaminophen overdose (n=8) compared to control healthy human liver. Explanted livers injured by acetaminophen overdose show expression of the senescence marker p21 detected by immunohistochemistry in residual hepatocytes surrounding areas of necrosis. Necrosis interface, dashed white line; CV, central vein; black asterisk indicates area of necrosis. As a control, human liver with normal histology was used (n= 50). Scale bar, 50μm. (**B**) A case series (n=74) of patients with sub-massive liver necrosis divided into subgroups according to the extent of hepatocellular necrosis, <25% n=8, 25-50% n=16, 50-75% n=22, >75% n= 28. The extent of hepatocellular submassive necrosis (defined histologically by globalized confluent necrosis) was quantified by immunohistochemistry for the hepatocellular senescence marker p16 and the proliferation marker Ki67. * = $p<0.05$, one way ANOVA. Mean ± SEM.

Europe PMC Funders Author Manuscripts

Europe PMC Funders Author Manuscripts

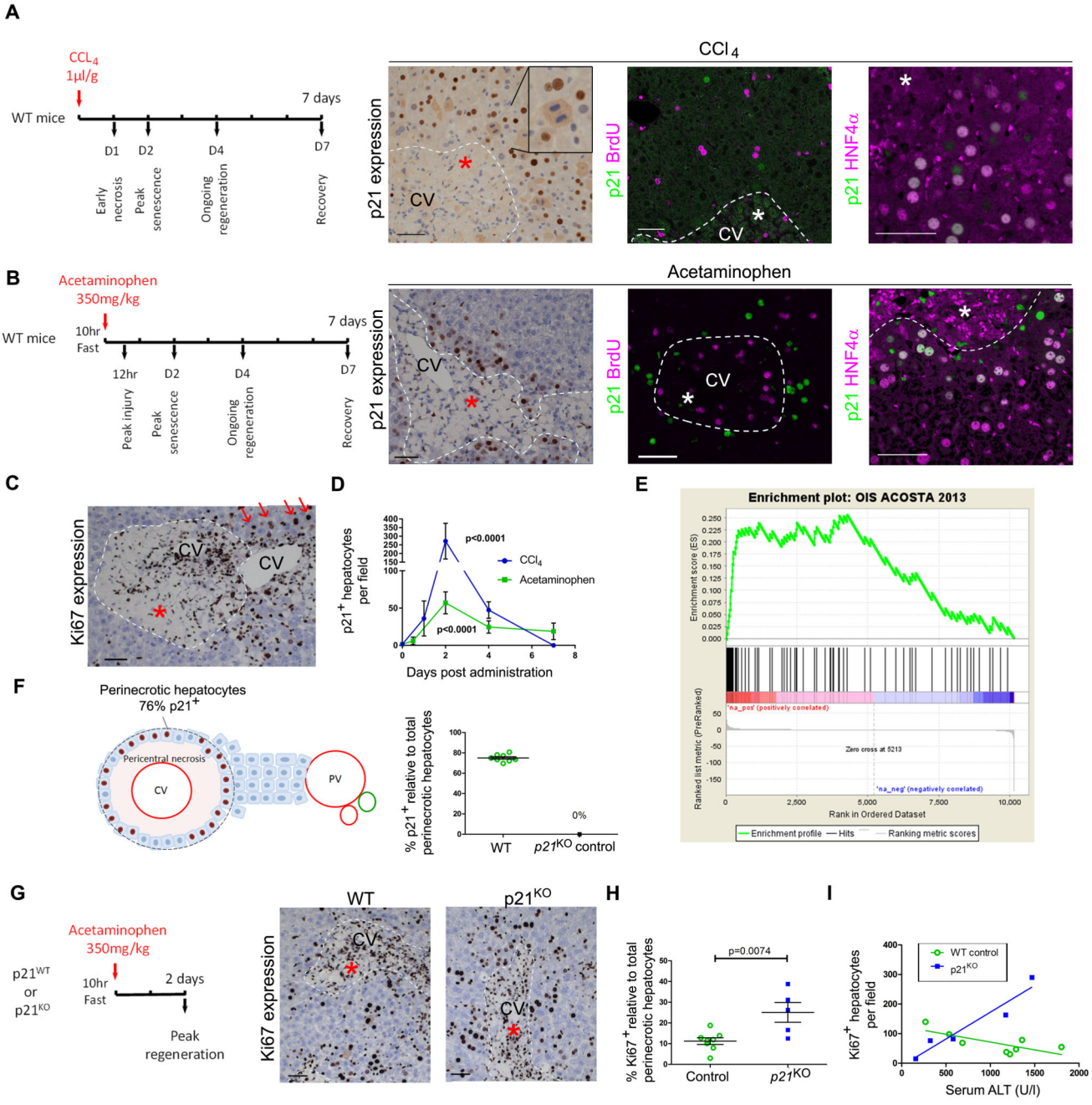

Fig. 2. Toxin-mediated liver injury causes p21-dependent hepatocellular senescence in mice.

(**A, B**) In murine toxin-induced acute liver injury models, mice were treated with either carbon tetrachloride (CCl_4) (**A**) or acetaminophen (**B**). Treatment with these toxins resulted in pericentral necrosis two days after administration as shown by immunohistochemistry for expression of the senescence marker p21, (green); also shown is expression of the proliferation marker BrdU (magenta) and the hepatocyte marker HNF4α (magenta). (**C**) Immunohistochemistry for expression of the proliferation marker Ki67 is shown two days after acetaminophen treatment. Staining indicates hepatocyte proliferation away from but not

next to the area of necrosis; red arrows, proliferating hepatocyte. (**D**) Quantification of $p21^{+}$ hepatocytes post injury; n≥3 for each time point, p value <0.0001 versus time = 0, two way ANOVA. (**E**) Gene Set Enrichment Analysis (GSEA) plot showing enrichment of the early (24 hours) acetaminophen injury gene expression signature in liver for an oncogene-induced senescence (OIS) signature. Geneset: IMR90 ER:RAS cell model (15). ES, enrichment score = 0.2564; NES, normalised enrichment score = 2.466; nominal p value <0.001. (**F**) Perinecrotic hepatocytes (brown nuclei) were quantified two days following acetaminophen for p21 expression; 74.9% of total perinecrotic hepatocytes expressed p21 (n=8 mice). (**G**) Immunohistochemistry for expression of the proliferation marker Ki67 in p21-deficient ($p21^{KO}$) mice two days after acetaminophen-induced liver injury. Ki67 expression indicates proliferating hepatocytes in the perinecrotic area of the injured mouse liver. (**H**) Quantification of perinecrotic hepatocytes in panel G. (**I**) Total $Ki67^{+}$ hepatocytes in relation to serum alanine transaminase (ALT; U/l), a marker of liver injury (n= 5 vs. 8 mice; 20 high power fields were quantified per liver. P = 0.0074, two-tailed t test. Linear regression for wildtype (WT) and $p21^{KO}$ mice R^2 0.54 and 0.92, with slope 95% confidence intervals -0.10 to -0.0045 and 0.082 to 0.28 and probability slope≠0, p = 0.037 and 0.010, respectively. Scale bars, 50μm. CV, central vein. Dashed white lines, necrosis boundary and asterisk, area of necrosis.

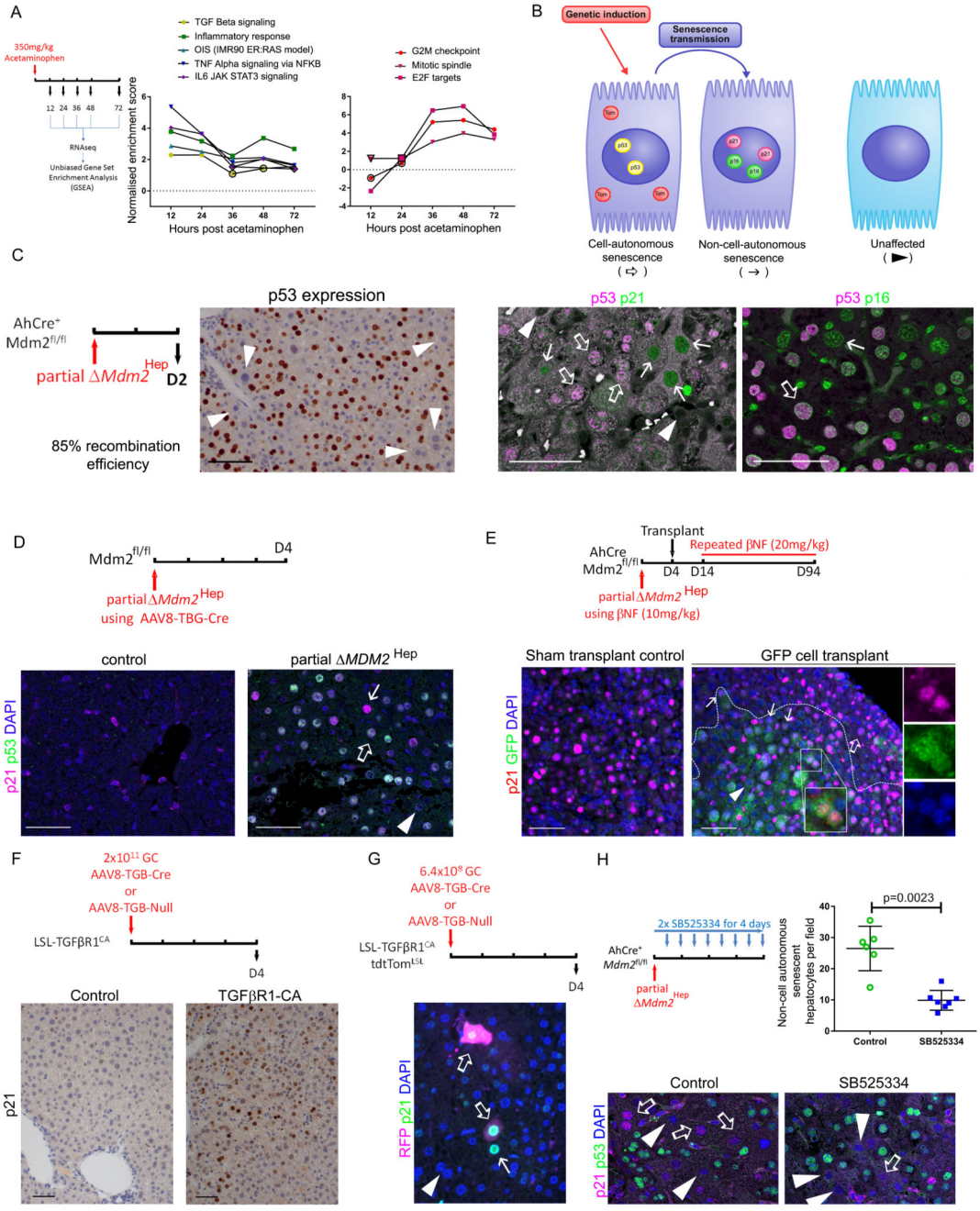

Fig. 3. Non-cell-autonomous senescence in hepatocyte-specific mouse senescence models.

(**A**) Plots of gene set enrichment analysis (GSEA) normalised enrichment scores comparing gene sets over time observed in the acetaminophen model to the unbiased top 15 ranked hallmarks gene sets and the oncogene-induced senescence (OIS) signature from IMR90 ER:RAS cell model (15), black borders of data points highlight p values <0.05; raw data is shown in Tables S2 and S3. Top and bottom panel present inflammatory and cell cycle arrest gene expression signatures. (**B**) Diagram showing the use of genetic induction of transgenes in hepatocytes to induce cell-autonomous senescence and assessment of senescence using a

combination of markers - p53, p21 and p16. Presence of senescence markers, p21 or p16, in the absence of markers of genetic recombination, p53 or Tomato reporter (Tom), identifies non-cell-autonomous senescence. (**C**) p53 accumulates in a subpopulation of hepatocytes in the partial Δ*Mdm2*^{Hep} mouse model where 20mg/kg β-naphthoflavone (βNF) is given to AhCre^{+} Mdm2$^{fl/fl}$ mice. Immunohistochemical staining for p21/p53 and for p53/p16^{INK4As} was assessed by confocal microscopy. (**D**) Immunohistochemical staining and confocal microscopic analysis of mouse liver sections for p53 and p21 after deletion of *Mdm2* using AAV8-TBG-Cre (2.5x10^{11} GC/mouse). (**E**) Immunohistochemical staining and confocal microscopic analysis of mouse liver sections for p21 expression and green fluorescent protein (GFP) staining in a hepatocyte transplant mouse model 94 days post transplantation of GFP tagged hepatocyte precursor cells. AhCre^{+} Mdm2$^{fl/fl}$ mouse recipients were given wildtype (WT) donor cells tagged with GFP and iterative doses of βNF to induce hepatocyte recombination of *Mdm2*. White dashed line, border of the engrafted cells. Magnified area is shown in individual color images on right. (**F**) Immunohistochemical staining and confocal microscopic analysis of mouse liver sections for p21 expression following hepatocellular TGFβR1 activation by AAV8-TBG-Cre in LSL-TGFβR1-CA mice. (**G**) Immunohistochemical staining and confocal microscopic analysis of mouse liver sections for p21 expression and red fluorescent protein (RFP) staining to detect tdTomato reporter after reduced dosing of the AAV8-TBG-Cre vector (6.4x10^{8} genetic copies per animal) in LSL-TGFβR1-CA R26-LSL-tdTomato mice. (**H**) Following partial Δ*Mdm2*^{Hep} mice were given the TGFβR1 inhibitor SB525334 or vehicle control. Immunohistochemical staining and confocal microscopic analysis of mouse liver sections for p53 and p21 with quantification of non-cell-autonomous p21 expression; p = 0.0023, two tailed Mann-Whitney test; n = 6 vehicle vs. 7 SB525334 treated mice. Mean ± SEM. Scale bars, 50μm. Open arrow, cell-autonomous senescence, closed arrow, non-cell-autonomous senescence, arrowhead, unaffected.

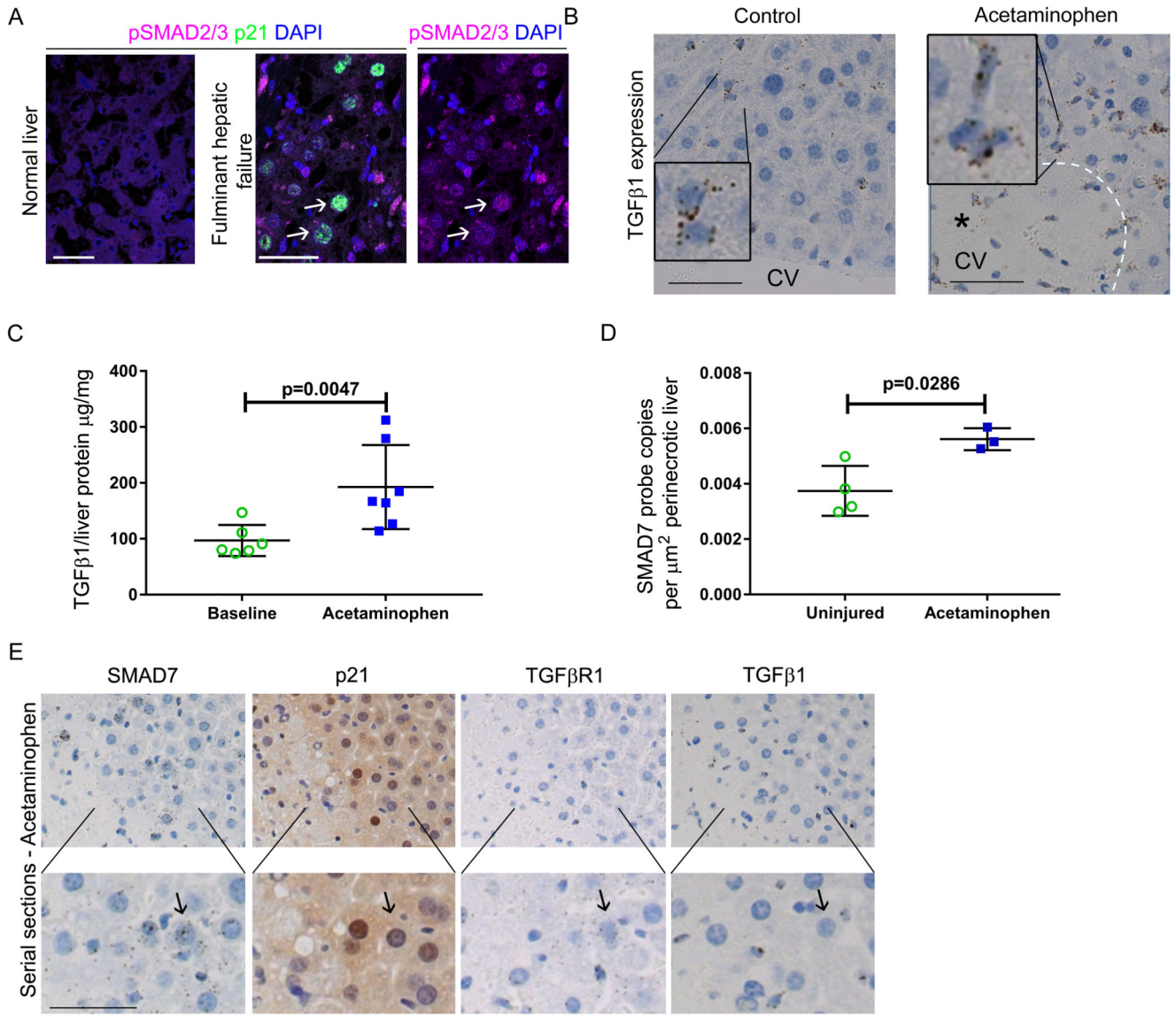

Fig. 4. TGFβ signaling is activated in acetaminophen-induced hepatocellular senescence.

(**A**) Representative images showing immunohistochemistry for expression of p21 and pSMAD2/3 in healthy human liver and in liver from patients with fulminant hepatic failure secondary to acetaminophen overdose. White arrows indicate senescent hepatocytes. (**B**) Representative images showing in situ hybridization for TGFβ1 in the liver of acetaminophen treated (350mg/kg) and untreated C57BL/6J mice. TGFβ1 ligand is expressed by non-parenchymal cells with a monocyte-like appearance. CV, central vein. Black asterisk indicates area of necrosis. (**C**) ELISA of mouse liver TGFβ1 in untreated and acetaminophen treated mice 12 hours after exposure. (n= 6 vs. 7, respectively). P=0.0047, two tailed Mann-Whitney. Mean ± SEM. (**D**) Quantification by in situ hybridization of SMAD7 expression in the perinecrotic region of mouse liver two days after acetaminophen treatment. P=0.0286, compared to equivalent area in uninjured mouse liver, one-tailed Mann-Whitney test. (**E**) Mouse liver serial sections assessed for expression of SMAD7,

TGFβR1 and TGFβ1 ligand by in situ hybridization and p21 by immunohistochemistry 12 hours after acetaminophen treatment. Scale bars, 50μm.

Europe PMC Funders Author Manuscripts

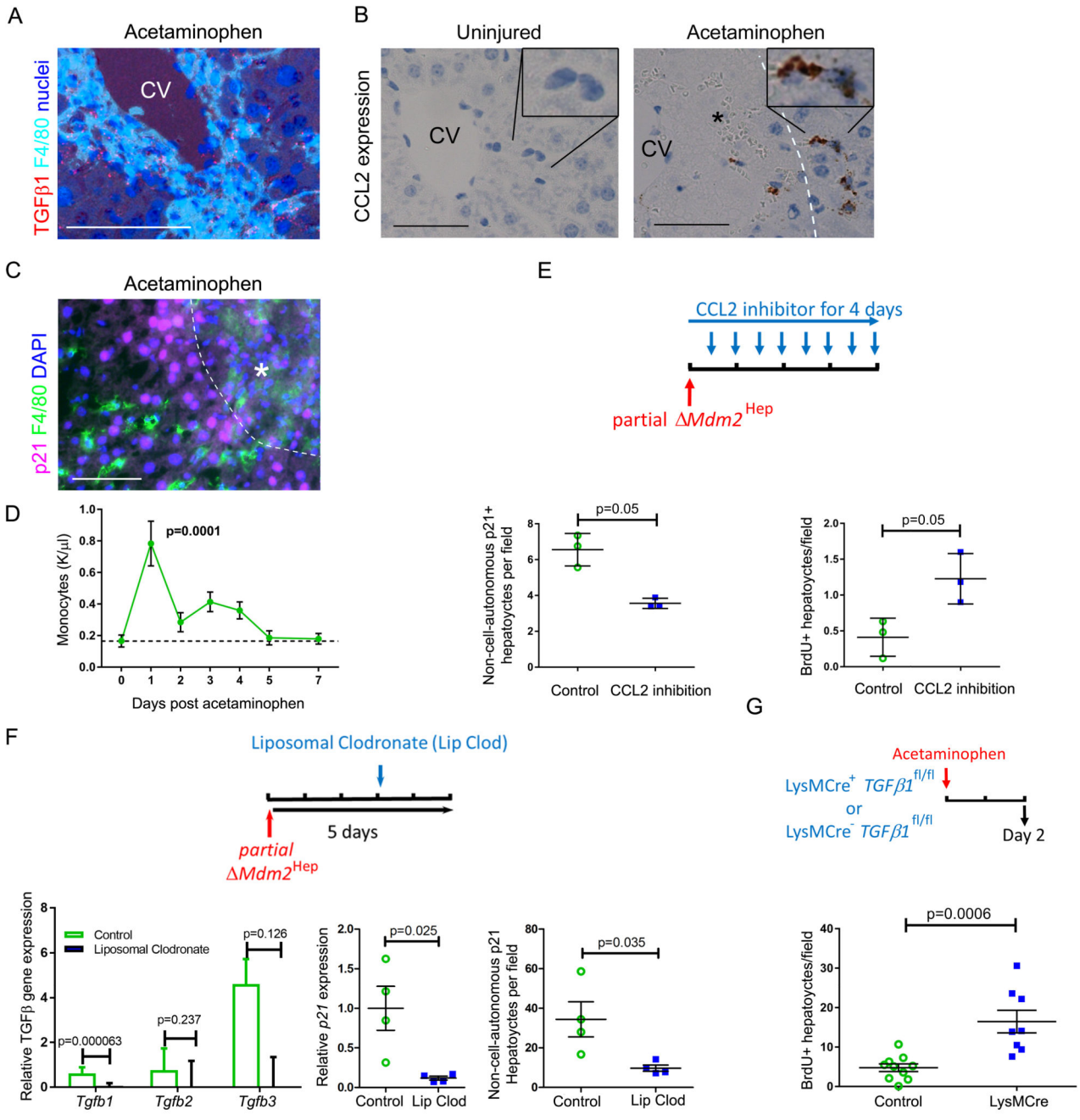

Fig. 5. Macrophage recruitment and TGFβ1 production drive hepatocellular senescence and impair hepatocellular regeneration in mice.

(**A**) Serial mouse liver sections assessed for hepatic TGFβ1 ligand production and F4/80^{+} macrophages by in situ hybridization and F4/80 immunohistochemistry respectively (two days after 350mg/kg acetaminophen). CV, central vein. (**B**) Shown is in situ hybridization staining for expression of the CCL2 chemokine. Dashed white line, necrotic interface, black asterisk, area of necrosis. (**C**) Immunohistochemical staining for F4/80^{+} macrophages and p21^{+} hepatocytes. Scale bars = 50μm. (**D**) Quantification of peripheral monocytes in mice

Europe PMC Funders Author Manuscripts

after acetaminophen treatment versus fasted untreated mice as baseline (dashed line). n = 5 mice for each time point. p = 0.0001, one way ANOVA with Dunnett's multiple comparison baseline vs. day one. (**E**) Immunohistochemical staining for p53 and p21 expression or for BrdU in livers four days after partial Δ*Mdm2*^{Hep}, where 20mg/kg β-naphthoflavone (βNF) is given to AhCre^{+} Mdm2$^{fl/fl}$ mice, followed by either twice daily antibody-mediated CCL2 inhibition or isotype antibody control. Non-cell-autonomous hepatocyte p21 expression (without p53 expression) and proliferation (BrdU) were quantified. p= 0.05, Mann-Whitney (n= 3 mice per group). (**F**) Liposomal clodronate depletion of macrophages three days after partial Δ*Mdm2*^{Hep} compared to PBS control. *TGFβ* ligands and *p21* expression in whole mouse liver were quantified by qRT-PCR. p values = 0.000063, 0.237, and 0.126 for TGFβ1, TGFβ2 and TGFβ3 respectively and 0.025 for p21, t test (n= 4 mice per group). Non-cell-autonomous p21^{+} hepatocytes were quantified after immunohistochemical staining for p53 and p21. P value = 0.035, t test (n= 4 mice per group). (**G**) Acetaminophen 350mg/kg was administered to *LysMCre*$^{+}$ *TGFβ*$^{fl/fl}$ or *LysMCre*^{WT} *TGFβ*$^{fl/fl}$ mouse littermates. Hepatocyte proliferation was assessed by BrdU immunohistochemistry. p=0.0006, two tailed t test (n= 10 vs. 8 mice). Mean ± SEM.

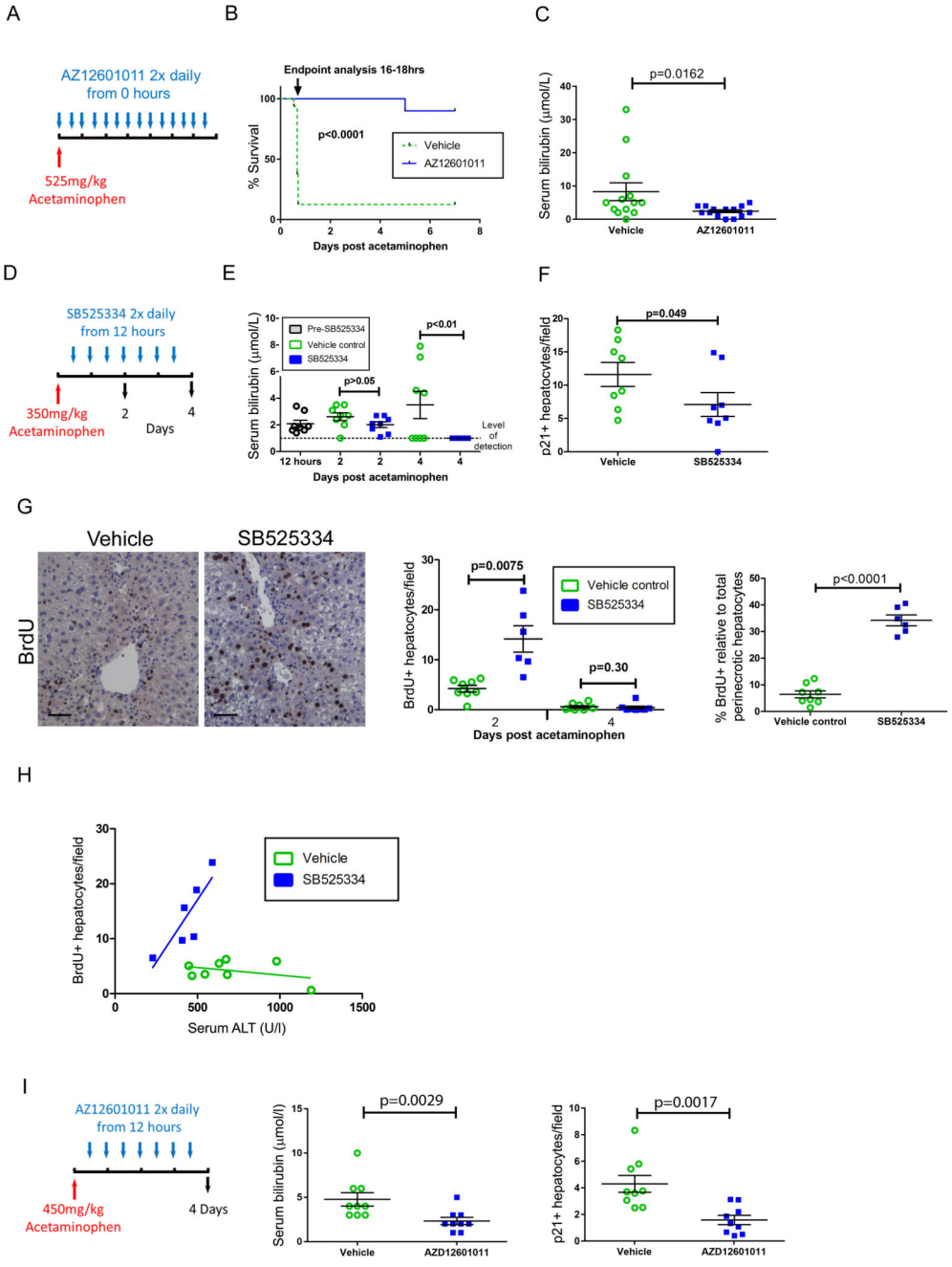

Fig. 6. Inhibition of TGFβR1 signaling reduces hepatocellular senescence and restores a proportional regenerative response after acetaminophen treatment in mice.

(**A**) Cohorts of male C57BL/6J mice were given vehicle control or were treated with the TGFβR1 inhibitor AZ12601011, starting when 525mg/kg acetaminophen was administered. Mice were closely monitored throughout until death or humane endpoint was reached, typically between 16 and 18 hours. Initially the mice treated with the TGFβR1 inhibitor (n = 14) were sacrificed when the control animals reached the endpoint irrespective of clinical condition (total biological replicates, n = 14 with AZ12601011 and n=16 with vehicle

Europe PMC Funders Author Manuscripts

control; performed over three separate experiments). (**B**) Separate survival cohorts (n = 5 in each of two experiments) treated with the TGFβR1 inhibitor were compared to simultaneous vehicle controls to examine longer term survival; p value < 0.0001, Gehan-Breslow-Wilcoxon test. (**C**) At matched endpoint, the TGFβR1 inhibitor and vehicle control groups were compared for serum bilirubin. P = 0.0162, two tailed Mann-Whitney. (**D**) In an experiment examining delayed TGFβR1 inhibition commencing 12 hours after acetaminophen treatment in male C57BL/6J mice the TGFβR1 inhibitor SB525334, or vehicle, was given twice daily. (**E**) Shown is serum bilirubin over time from panel D; p >0.05 and <0.01 at days two and four for SB525334 treatment compared to vehicle control respectively, two way ANOVA with Bonferroni correction (n= 8 each group). (**F**) Immunohistochemical staining for hepatocellular p21 expression was quantified; p= 0.049, t test, 30 high power fields of liver were analyzed, n=8 mice per group. (**G**) Shown is immunohistochemical staining for hepatocellular BrdU (representative images for two day post acetaminophen time point are shown) for both whole liver and perinecrotic hepatocytes (day two only). P values = 0.0075, and 0.30 for total BrdU+ hepatocytes at days 2 and 4 respectively and <0.0001 for BrdU+ perinecrotic hepatocytes comparing SB525334 treatment to vehicle control, t test (groups n= 8 each, except day 2 vehicle where n=6). Scale bars, 50μm. (**H**) In individual mice, two days post acetaminophen treatment, hepatocytes were analyzed for serum ALT and BrdU staining and linear regression was performed. R^2 0.15 and 0.71, with Slope 95% confidence intervals -0.0094 to 0.0038 and 0.0049 to 0.085 and probability slope ≠ 0, p = 0.34 and 0.036, respectively. (**I**) A non-fatal dose of acetaminophen (450mg/kg) was administered to male C57BL/6J mice, followed by treatment with AZ12601011 or vehicle control twelve hours later. Serum bilirubin was measured and p21 expression in hepatocytes was quantified by immunohistochemistry. P = 0.0029 and 0.0017 respectively comparing AZ12601011 treatment to vehicle control, two tailed t test, n=9 per group. Data presented as mean ± SEM.